Journal of Astronomical Telescopes, Instruments, and Systems

AstronomicalTelescopes.SPIEDigitalLibrary.org

Solution uniqueness and noise impact in a static spectropolarimeter based on birefringent prisms for full Stokes parameter retrieval

Bogdan Vasilescu
Yaël Nazè
Jérôme Loicq

SPIE.

Bogdan Vasilescu, Yaël Nazè, Jérôme Loicq, "Solution uniqueness and noise impact in a static spectropolarimeter based on birefringent prisms for full Stokes parameter retrieval," *J. Astron. Telesc. Instrum. Syst.* **6**(2), 028001 (2020), doi: 10.1117/1.JATIS.6.2.028001

Solution uniqueness and noise impact in a static spectropolarimeter based on birefringent prisms for full Stokes parameter retrieval

Bogdan Vasilescu,[a,*] Yaël Nazè,[b] and Jérôme Loicq[a]
[a]Université de Liège, Centre Spatial de Liège, Liège, Belgium
[b]Université de Liège, Liège, Belgium

Abstract An innovative model of a static spectropolarimeter able to cover the entire Stokes vector is discussed. The optical layout is based on a birefringent modulator formed by two antiparallel prisms stuck together with the help of an intermediary part of the same material. This optical model has the advantage of being extremely compact. It avoids any movable parts or rotating components. By its architecture, the device induces a complete modulation on the vertical direction of any incoming polarized light, facilitating the determination of the entire Stokes vector through a single measurement. Because the modulation is also wavelength-dependent, spectral dependencies of the polarization states can be derived. The behavior of the model was first investigated in noise-free conditions. The existence of a unique solution was proven in the absence of noise and for any Stokes vector configuration. Under noisy conditions, the uncertainty on the Stokes parameters and the efficiency of the modulation scheme were evaluated as a function of the analyzer's angle and for two different configurations of the modulator. The simulations show that an almost ideal efficiency is reachable, qualifying the concept for the high-precision measurement of the polarization. [DOI: 10.1117/1.JATIS.6.2.028001]

Keywords: optics; polarimetry; spectropolarimetry; birefringence; modulation scheme; efficiency of modulation.

Paper 19129 received Dec. 19, 2019; accepted for publication Apr. 7, 2020; published online Apr. 23, 2020.

1 Introduction

The study of the polarization of light is an excellent way to get information about remote objects. Measuring this property leads to gathering essential information about the environment and the optical sources. In astronomy, for instance, with the help of the Zeeman or Hanle effect, the polarization becomes the best method to determine the magnetic field of stars.[1,2] Moreover, during the last years, polarimetry has also been found to be a possible interesting tool for the detection and study of exoplanets.[3–5]

With scattering theories, the polarization also brings information about the size, the shape, and the distribution of scattering particles, helping to characterize the surface or the atmosphere of astronomical bodies.[1,2,5] Combining polarization with spectral properties, the collected data become even more important for the description of the medium. Moreover, the applicability of the polarization goes far beyond astronomy. Chemistry, biology, and medicine are also making extensive use of this technique. Generally, the instruments used for polarization determination are based on a modulator (which can be a polarizer, a phase shifter, or a rotator) and a polarizer (analyzer). The role of the modulator is to convert any incoming state of polarization into a predetermined type of polarization, which will then be studied with the help of the analyzer. Because most of the detectors (such as CCD, CMOS, etc.) are only sensitive to light intensity, the structure of the polarimeter must convert the parameters relative to the polarization of light (Stokes parameters) onto a level of detected intensity.[6,7]

*Address all correspondence to Bogdan Vasilescu, E-mail: bvasilescu@uliege.be

2329-4124/2020/$28.00 © 2020 SPIE

It can be proven that the measured intensity depends both on the phase difference induced by the modulator and on the orientation of the analyzer.[8] In the past, two significant families of measurement techniques have been developed to evaluate the polarization states of light: one using rotating components and another using amplitude division.

In the first case, by varying the relative position of the analyzer and the modulator, a sequential (or temporal) modulation of the measured intensity is obtained. At least, four different configurations are required to determine all four Stokes parameters describing the polarization of the light. The second technique, which is static, is based on the use of birefringent elements such as Wollaston prisms, Babinet compensators, and Glan–Foucault prisms. In this way, precise modulations of the light intensity can be obtained at different positions in space with regard to the optical path of the incoming ray.

Thereby, the determination of the polarization can follow either a discrete method, either a continuous one, according to the number of modulations received by the outgoing intensity of light, and used to compute the incoming polarization. Most of the time, both measurement procedures occupy a relatively large volume and make use of complex mechanisms. The considerable dimensions and the need for rotating parts are the most significant drawbacks for the space usage of these classical types of polarimeters. Indeed, they directly impact the cost, the design, and the safety of space missions.

In this context, the methodology proposed by Sparks[9] and further developed by Pertenais et al.[10] for single-shot full Stokes polarimetry has the advantage of being extremely compact and robust, without any moving components.

The originality of this concept, hereafter referred to as STAS (static spectropolarimeter), is based on the modulation of the incoming signal due to the chromatic birefringence of the modulator $\Delta n(\lambda)$ combined with a specific geometry of the device.[10,11] Any incoming polarization state will acquire a continuous modulation depending simultaneously on the wavelength and the position. The concept can be used on a large wavelength range by choosing an appropriate material for the modulator. For instance, the use of magnesium fluoride (MgF_2) gives access to the entire spectrum between 0.12 and 7 μm,[12,13] whereas with calcium fluoride the working window is even larger, from 0.13 to 9.7 μm.[14,15] Because of the wavelength dependence of the modulation characterizing the received intensity, the instrument can be converted into a spectropolarimeter only by placing a spectrometer after the analyzer.

The key part of the design is the modulator, formed by two antiparallel birefringent uniaxial wedges, with fast axes oriented at 45 deg one about another (see Fig. 1). By continuously varying the phase difference between the orthogonal components of light, the first wedge will modulate along the vertical direction any incoming state of polarization, except the Q state. This one will pass unaffected because the optical axis is oriented along the x direction (see Fig. 1). A second birefringent wedge, having the fast axis at 45 deg with respect to x direction will drastically simplify the computations and will lift the Q state degeneracy.

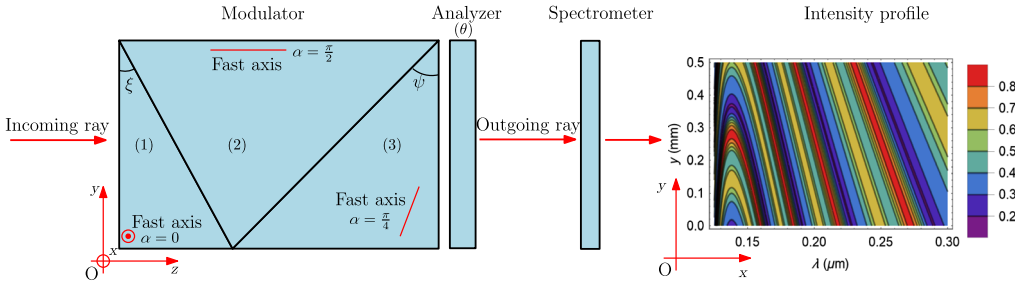

Fig. 1 The incoming light arriving from the left-hand side is collimated and perpendicular to the surface of the instrument, the (xy plane). After passing through the polarimeter, the emerging light has an intensity modulated along the vertical direction (along the y axis). The spectrometer then leads to a wavelength dispersion along the horizontal direction (x axis). The observed intensity profile represented here corresponds to an arbitrary state of polarization $\mathbf{S} = [1, 0.4, 0.3, 0.5]^{\mathsf{T}}$ and to a modulator build in MgF_2, with the apex angles $\xi = 1.5$ deg and $\psi = 3$ deg. The orientation of the analyzer was $\theta = 90$ deg. Additionally, it was considered that the entire incoming beam is identically polarized, being characterized by a single polarization state, i.e., the vector $\mathbf{S}$.

In this paper, we discuss three questions on this new concept of a spectropolarimeter. First, the uniqueness of the solution: we demonstrate in Sec. 3 that in the ideal conditions of the absence of noise, any pattern of the intensity from the detector plane is associated with a single state of polarization.

The second question concerns the quality of the measurement under noisy circumstances. What is the precision of this instrument when the noise is present? The answer to this question is detailed in Sec. 4.

The third question is related to the efficiency of the modulation scheme, as it was defined by del Toro Iniesta.[8] We study it in Sec. 5 for different orientations of the analyzer, different apex angles, and various modulation schemes. Answering this question allows us to compare the model with other existing instruments and to find an optimal architecture.

2 Static Spectropolarimeter Concept

The key part of STAS is the modulator based on three birefringent uniaxial elements made of the same material (Fig. 1). Two antiparallel wedges [parts (1) and (3) in Fig. 1] of very small apex angles ξ and ψ are optically glued together with the help of a third piece placed in between [element (2)]. The fast axis has a specific orientation in each component of the modulator: parallel to the x axis in the first wedge, parallel to z axis in the middle part and at 45 deg with regard to x axis [in the (xy) plane] in the last wedge.[9,10,16]

In addition to the modulator, the polarimeter needs a linear polarizer (or analyzer), oriented at an angle θ about the x axis, in the plane (xy). After the passage through the polarimeter, the light is spectrally dispersed by the spectrometer over the x axis.

2.1 *Working Principle*

The description of the polarization is performed with the Stokes formalism. According to this, the information about polarization is encoded into the Stokes vector:

$$\mathbf{S} = \begin{bmatrix} I \\ Q \\ U \\ V \end{bmatrix}. \tag{1}$$

Its components have the dimension of intensity and are associated with specific types of polarization of the incident light.[7] I represents the total intensity, Q is the linear horizontal or vertical polarization, and U is the linear polarization at 45 deg or 135 deg, whereas V is the circular left or right polarization:

$$\begin{cases} I = E_{0x}^2 + E_{0y}^2 \\ Q = E_{0x}^2 - E_{0y}^2 \\ U = 2E_{0x}E_{0y}\cos\epsilon \\ V = 2E_{0x}E_{0y}\sin\epsilon \end{cases}. \tag{2}$$

Under this notation, E_{0x} and E_{0y} are the amplitudes associated with the orthogonal components of the electric field of light, and ϵ is the phase difference between these components. Another useful notion is the degree of polarization:

$$p = \frac{\sqrt{Q^2 + U^2 + V^2}}{I}, \quad 0 \le p \le 1, \tag{3}$$

with $p = 1$ in the case of the totally polarized light and $p = 0$ for the nonpolarized light. In a more detailed definition, the degree of linear polarization is given by $p_{\text{lin}} = \sqrt{Q^2 + U^2}/I$ while the degree of circular polarization is $p_{\text{circ}} = V/I$.

To deal with the passage through an optical element like the modulator or the analyzer, the Mueller calculus is used. Principles of this state that to any polarizing element one may associate a Mueller matrix $\mathbf{M}$, 4×4, such as

$$\mathbf{S}_{\text{out}} = \mathbf{M} \cdot \mathbf{S}_{\text{in}}, \tag{4}$$

where $\mathbf{S}_{\text{out}}$ is the Stokes vector of the outgoing polarization, after its travel through the instrument, and $\mathbf{S}_{\text{in}}$ is the incoming polarization. Every subelement of the optical assembly is represented by its Mueller matrix, giving the combination:

$$\mathbf{M} = \mathbf{M}_n \cdot \mathbf{M}_{n-1} \cdot \ldots \cdot \mathbf{M}_1, \tag{5}$$

where $\mathbf{M}_n$ is the last element crossed by light.

Based on this formalism, we analyze in this section each component of the modulator, emphasizing the need for a triple structure.

2.2 *Single Wedge and Analyzer*

Being composed of a birefringent uniaxial material with the fast axis oriented along the x axis, the first element acts as a variable waveplate (see Fig. 2).

Indeed, because the distance travelled by the light inside the wedge decreases upward, the phase difference ($\Delta\phi_1$) varies linearly with y following the relation:

$$\Delta\phi_1 = \frac{2\pi}{\lambda}\Delta n(\lambda)(h - y)\tan\,\xi, \tag{6}$$

where λ is the wavelength of the incoming light, $\Delta n(\lambda) = |n_o(\lambda) - n_e(\lambda)|$ is the absolute value of the difference between the ordinary and the extraordinary indices of refraction of the element (1), h is the height of the wedge, y is the position on the vertical axis of the incidence point for the incoming ray, and ξ is the apex angle. Due to this geometry, periodically, at certain levels along the y axis, the phase difference will embrace particular values such as $\frac{\pi}{2}$, π, or 2π. At these precise positions, the wedge will behave like a quarter-wave plate, half-wave plate, and full-wave plate, respectively. Because of this, any incoming homogeneous state of polarization, described by

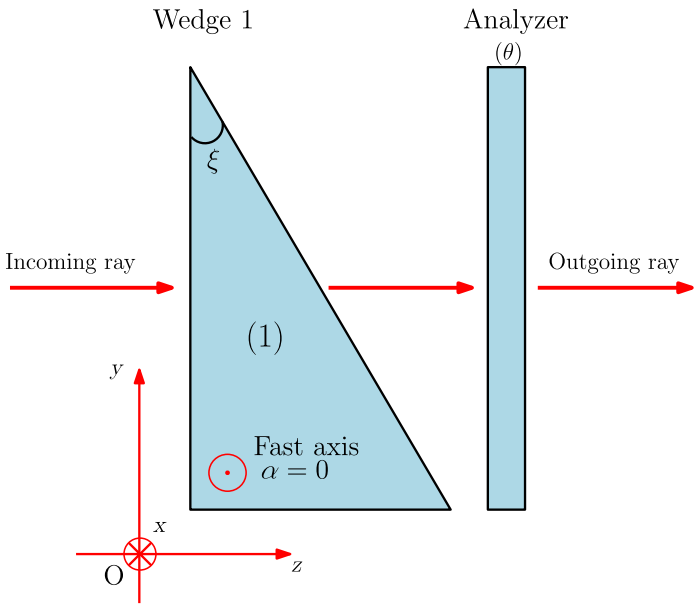

Fig. 2 General representation of the first block, (1), followed by an analyzer. The fast axis of the element (1) is oriented along the x axis. The analyzer, which is a linear polarizer, has its optical axis oriented at an angle θ with respect to the same x direction, in the (xy) plane.

Eq. (2), will see its U and V parameters varying along the vertical. Given the orientation of the fast axis in the first wedge, the Q term cannot be affected by this polarizing element. Any incoming linear polarization, horizontal or vertical, is passing through the system without changes. A comprehensive representation of the transformations endured by light travelling through the instrument is obtained via the Mueller calculus. The general Mueller matrix of a rotated waveplate [with a rotation angle α with regard to the x axis, in the (xy) plane] is given by[7]

$$\mathbf{M} = \begin{bmatrix} 1 & 0 & 0 & 0 \\ 0 & c^2 + s^2 \cos \Delta\phi & (1 - \cos \Delta\phi)cs & s \sin \Delta\phi \\ 0 & (1 - \cos \Delta\phi)cs & s^2 + c^2 \cos \Delta\phi & -c \sin \phi \\ 0 & -s \sin \Delta\phi & c \sin \Delta\phi & \cos \Delta\phi \end{bmatrix}, \tag{7}$$

where $c = \cos 2\alpha$, $s = \sin 2\alpha$, and $\Delta\phi$ is the phase difference induced by the birefringent medium between the ordinary and the extraordinary rays. Because in the present case $c = 1$, $s = 0$, the corresponding Mueller matrix can be easely computed. The Mueller matrix of an analyzer oriented at an angle θ is given by[7]

$$\mathbf{M_A}(\theta) = \frac{1}{2} \begin{pmatrix} 1 & c & s & 0 \\ c & c^2 & cs & 0 \\ s & cs & s^2 & 0 \\ 0 & 0 & 0 & 0 \end{pmatrix}, \tag{8}$$

in which the notation $c = \cos 2\theta$, $s = \sin 2\theta$ was again adopted for θ the angle between the optical axis of the polarizer and the positive x axis, in the (xy) plane.

Using Eqs. (7) and (8) and the general rules for the Mueller calculus [Eqs. (4) and (5)], we find the outgoing Stokes vector $\mathbf{S}_{\text{out}}$ corresponding to an incoming polarization $\mathbf{S}_{\text{in}} = [I_{\text{in}}, Q_{\text{in}}, U_{\text{in}}, V_{\text{in}}]^{\text{T}}$:

$$\mathbf{S}_{\text{out}}(\theta, y, \lambda) = \frac{1}{2} \begin{pmatrix} I_{\text{in}} + Q_{\text{in}}c + U_{\text{in}}s \cos \Delta\phi_1 - V_{\text{in}}s \sin \Delta\phi_1 \\ cI_{\text{in}} + Q_{\text{in}}c^2 + U_{\text{in}}cs \cos \Delta\phi_1 - V_{\text{in}}cs \sin \Delta\phi_1 \\ I_{\text{in}}s + Q_{\text{in}}cs + U_{\text{in}}s^2 \cos \Delta\phi_1 - V_{\text{in}}s^2 \sin \Delta\phi_1 \\ 0 \end{pmatrix}. \tag{9}$$

This vector depends on the orientation of the analyzer through $c = \cos 2\theta$ and $s = \sin 2\theta$, on the position on the vertical direction of the incidence point of the incoming ray (y) and of the wavelength of this ray (λ). For a static design, the angle θ is fixed. The first term of the vector is the outgoing intensity, which can be measured by a detector. In the present case, we have

$$I_{\text{out}}(\theta, y, \lambda) = \frac{1}{2}(I_{\text{in}} + Q_{\text{in}}c + U_{\text{in}}s \cos \Delta\phi_1 - V_{\text{in}}s \sin \Delta\phi_1). \tag{10}$$

Taking measurements of the intensity at different positions along the y axis and at a given wavelength, one finds different values, because of the phase difference variation $(\Delta\phi_1)$. Nevertheless, no matter the number of equations that are obtained for different values of the phase, the I_{in} and Q_{in} terms cannot be determined from this configuration of the polarimeter. In any system of equations that is build, the columns corresponding to I_{in} and Q_{in} are just multiple of one another. The only solution to this problem is to insert a second wedge between the first one and the analyzer. If the fast axis of this second birefringent element is oriented in a different way with respect to the first, then the Q state will also acquire a modulation, and the systems of equations that can be build to express the outgoing intensity become entirely determined.

2.3 *Compound Structure*

The best architecture able to ensure a full modulation of the Stokes parameters then has the form presented in Fig. 1. A second wedge [element (3) in Fig. 1] of apex angle ψ and antiparallel to the first one is added along the light path. In order to ensure the stiffness of the compound and

a homogeneous index of refraction so that the deviation of light to be minimized, an intermediary element [labeled with (2) in Fig. 1] is placed in between. This middle part of the polarimeter plays no role in the modulation of light. Indeed, since the fast axis lies along the z axis ($\alpha = \frac{\pi}{2}$), the ordinary and extraordinary rays are traveling at the same speed along the z axis, and because of this, the phase difference is constant for any position along the vertical axis. The Mueller matrix of the element (2) is then the identity matrix, 1. Considering that the element (3) has a fast axis oriented at an angle $\alpha = \frac{\pi}{4}$ with respect to the x axis in the (xy) plane, the phase difference acquired here is $\Delta\phi_3 = \frac{2\pi}{\lambda}\Delta n(\lambda)(h-y)\tan\psi$, and then, with the help of the Eqs. (7) and (8), the Mueller matrix of the entire birefringent block can be calculated. The reason for choosing $\alpha = \frac{\pi}{4}$ is mostly related to simplification of computations, this value ensuring an elegant form for the Muller matrix of the element (3). Multiplying this matrix with the Stokes vector of the incoming light, $\mathbf{S}_{\text{in}} = [I_{\text{in}}, Q_{\text{in}}, U_{\text{in}}, V_{\text{in}}]^{\text{T}}$, the outgoing Stokes vector can be obtained

$$\mathbf{S}_{\text{out}}(\theta, y, \lambda) = \frac{1}{2}\begin{bmatrix} I_{\text{in}} + Q_{\text{in}}cc_3 + U_{\text{in}}(sc_1 + cs_1s_3) + V_{\text{in}}(cc_1s_3 - ss_1) \\ I_{\text{in}}c + Q_{\text{in}}c^2c_3 + U_{\text{in}}(csc_1 + c^2s_1s_3) + V_{\text{in}}(c^2c_1s_3 - css_1) \\ I_{\text{in}}s + Q_{\text{in}}csc_3 + U_{\text{in}}(s^2c_1 + css_1s_3) + V_{\text{in}}(csc_1s_3 - s^2s_1) \\ 0 \end{bmatrix}, \tag{11}$$

where the following contracted notations were used

$$\begin{aligned} c &= \cos 2\theta \quad & s &= \sin 2\theta \\ c_1 &= \cos \Delta\phi_1 \quad & s_1 &= \sin \Delta\phi_1 \\ c_3 &= \cos \Delta\phi_3 \quad & s_3 &= \sin \Delta\phi_3. \end{aligned}$$

The terms c and s are constants as they describe the orientation of the analyzer, which is considered fixed. However, the terms c_1, s_1 and c_3, s_3 are variables, depending simultaneously on the vertical position and on the wavelength. The intensity measured by a detector placed after this polarimeter is given by the first element of the vector [Eq. (11)]:

$$I_{\text{out}}(\theta, y, \lambda) = \frac{1}{2}[I_{\text{in}} + Q_{\text{in}}cc_3 + U_{\text{in}}(sc_1 + cs_1s_3) + V_{\text{in}}(cc_1s_3 - ss_1)]. \tag{12}$$

In order the simplify further calculations, an even more contracted form of the outgoing intensity can be employed:

$$I_{\text{out}}(\theta, y, \lambda) = \frac{1}{2}[I_{\text{in}} + Q_{\text{in}} \cdot m(\theta, y, \lambda) + U_{\text{in}} \cdot n(\theta, y, \lambda) + V_{\text{in}} \cdot p(\theta, y, \lambda)], \tag{13}$$

where

$$\begin{cases} m(\theta, y, \lambda) = \cos(2\theta)\cos\Delta\phi_3 \\ n(\theta, y, \lambda) = \sin(2\theta)\cos\Delta\phi_1 + \cos(2\theta)\sin\Delta\phi_1\sin\Delta\phi_3 \\ p(\theta, y, \lambda) = \cos(2\theta)\cos\Delta\phi_1\sin\Delta\phi_3 - \sin(2\theta)\sin\Delta\phi_1 \end{cases}. \tag{14}$$

The new architecture of the polarimeter ensures the modulation of the Q parameter, with the help of the term $\cos\Delta\phi_3$ from the $m(\theta, y, \lambda)$ function. Reading the intensity at different vertical positions, a given wavelength (i.e., at a given horizontal position) and with a fixed orientation of the analyzer, a system of equations can be built

$$\begin{cases} I_{\text{out}}(y_1) = \frac{1}{2}[I_{\text{in}} + Q_{\text{in}} \cdot m(y_1) + U_{\text{in}} \cdot n(y_1) + V_{\text{in}} \cdot p(y_1)] \\ I_{\text{out}}(y_2) = \frac{1}{2}[I_{\text{in}} + Q_{\text{in}} \cdot m(y_2) + U_{\text{in}} \cdot n(y_2) + V_{\text{in}} \cdot p(y_2)] \\ I_{\text{out}}(y_3) = \frac{1}{2}[I_{\text{in}} + Q_{\text{in}} \cdot m(y_3) + U_{\text{in}} \cdot n(y_3) + V_{\text{in}} \cdot p(y_3)] \\ I_{\text{out}}(y_4) = \frac{1}{2}[I_{\text{in}} + Q_{\text{in}} \cdot m(y_4) + U_{\text{in}} \cdot n(y_4) + V_{\text{in}} \cdot p(y_4)] \\ . \\ . \end{cases}. \tag{15}$$

This system allows us to determine the polarization state of the incoming light and represents the modulation scheme of the polarimeter. However, given the complexity of the functions m, n, and p and the arbitrary number of equations, the uniqueness of the solution for the system [Eq. (15)] has to be proven.

3 Uniqueness of the Solution

To validate this configuration, the ability of the STAS to distinguish different incoming polarization states must be demonstrated. In other words, we have to prove that any incoming Stokes vector gives rise to a unique intensity profile. We use a "reductio ad absurdum" method: let us suppose that, for at least one wavelength, there exist two incoming Stokes vectors $\mathbf{S}_{\text{in1}}$ and $\mathbf{S}_{\text{in2}}$ providing the same intensity pattern I_{out} on the detector plane

$$\begin{cases} \mathbf{S}_{\text{in1}} \neq \mathbf{S}_{\text{in2}} \\ I_{\text{out1}}(y) = I_{\text{out2}}(y), \text{ for at least one } \lambda \text{ and } \forall\ y, \end{cases} \tag{16}$$

where $\mathbf{S}_{\text{in1}} = [I_1, Q_1, U_1, V]_1^{\text{T}}$ and $\mathbf{S}_{\text{in2}} = [I_2, Q_2, U_2, V_2]^{\text{T}}$, whereas $I_{\text{out1}}(y)$ and $I_{\text{out2}}(y)$ are the received intensities for a given wavelength [Eq. (13)]. Therefore:

$$\begin{cases} I_{\text{out1}}(y) = \frac{1}{2}[I_1 + Q_1 \cdot m(y) + U_1 \cdot n(y) + V_1 \cdot p(y)] \\ I_{\text{out2}}(y) = \frac{1}{2}[I_2 + Q_2 \cdot m(y) + U_2 \cdot n(y) + V_2 \cdot p(y)] \end{cases}, \tag{17}$$

where $m(y)$, $n(y)$, $p(y)$ are the functions defined in Eq. (14) for the considered wavelength, and driven only by the instrumental parameters.

Combining Eqs. (16) and (17), we then find that

$$\Delta I + \Delta Q \cdot m(y) + \Delta U \cdot n(y) + \Delta V \cdot p(y) = 0, \quad \text{for at least one } \lambda \text{ and } \forall\, y, \tag{18}$$

where $\Delta I = I_2 - I_1$, $\Delta Q = Q_2 - Q_1$, $\Delta U = U_2 - U_1$, and $\Delta V = V_2 - V_1$.

A combination $(\Delta I, \Delta Q, \Delta U, \Delta V)$ different from (0, 0, 0, 0) satisfying this last relation for any value of y and for at least one wavelength exists only if the functions $[1, m(y,\lambda), n(y,\lambda), p(y,\lambda)]$ are linearly dependent. To test this hypothesis, the mathematical theorem of the Wronskian is used.[17,18] According to this, if for a set of functions $f_i(y)$, $i = 1,2,\ldots,n$ which are $n-1$ times differentiable on an interval $[a,b]$, we have

$$\mathbf{W}[f_1(y), f_2(y), f_3(y), \ldots, f_n(y)] = \begin{vmatrix} f_1(y) & f_2(y) & f_3(y) & \cdots & f_n(y) \\ \frac{df_1(y)}{dy} & \frac{df_2(y)}{dy} & \frac{df_3(y)}{dy} & \cdots & \frac{df_n(y)}{dy} \\ \frac{d^2f_1(y)}{dy^2} & \frac{d^2f_2(y)}{dy^2} & \frac{d^2f_3(y)}{dy^2} & \cdots & \frac{d^2f_n(y)}{dy^2} \\ \cdots & \cdots & \cdots & \cdots & \\ \frac{d^{n-1}f_1(y)}{dy^{n-1}} & \frac{d^{n-1}f_2(y)}{dy^{n-1}} & \frac{d^{n-1}f_3(y)}{dy^{n-1}} & \cdots & \frac{d^{n-1}f_n(y)}{dy^{n-1}} \end{vmatrix} = 0 \tag{19}$$

$$\forall\ y \in [a,b],$$

then the functions are linearly dependent. Thus if there exists $y \in [a,b]$ such as $\mathbf{W}[f_1(y), f_2(y), \ldots] \neq 0$, then the functions are independent.[17,18] In the present case, for any given λ, the Wronskian can be expressed as

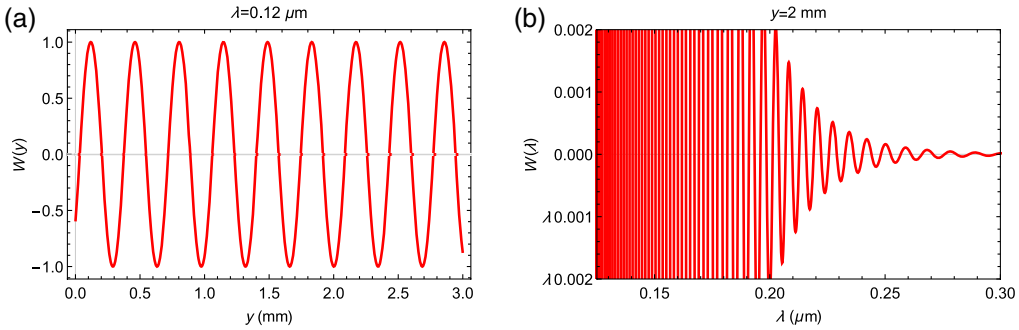

Fig. 3 Variation of the normalized Wronskian determinant. The behavior with respect to (a) y is shown for $\lambda = 0.12$ μm and (b) $y = 2$ mm. To simplify the computation of $W[1, m(\lambda), n(\lambda), p(\lambda)]$, a constant birefringence of the medium was assumed, of $\Delta n = 0.0132$, corresponding to the mean value of the birefringence of MgF_2 between 0.12 and 0.4 μm. For the legibility of the graphic, only the UV part of the spectrum was represented here. Also for the simplicity of computation, the orientation of the analyzer was chosen to be $\theta = 90$ deg.

$$\mathbf{W}[1, m(y), n(y), p(y)] = \begin{vmatrix} 1 & m(y) & n(y) & p(y) \\ 0 & \frac{dm(y)}{dy} & \frac{dn(y)}{dy} & \frac{dp(y)}{dy} \\ 0 & \frac{d^2m(y)}{dy^2} & \frac{d^2n(y)}{dy^2} & \frac{d^2p(y)}{dy^2} \\ 0 & \frac{d^3m(y)}{dy^3} & \frac{d^3n(y)}{dy^3} & \frac{d^3p(y)}{dy^3} \end{vmatrix} \quad \forall\, y \in [0, h], \tag{20}$$

where h is the height of the instrument. Meanwhile, in order to eliminate the possibility to obtain $\mathbf{W}[1, m(y), n(y), p(y)] = 0$ because of the inappropriate choice of the wavelength, the determinant $\mathbf{W}[1, m(\lambda), n(\lambda), p(\lambda)]\ \forall\ \lambda$ must also to be calculated for an arbitrary value of y. Both determinants are plotted with regard to y and λ (Fig. 3). Because the functions $m(y, \lambda)$, $n(y, \lambda)$, and $p(y, \lambda)$ depend on the parameters of the system, a structure on MgF_2, with apex angles $\xi = 1.5$ deg, $\psi = 3$ deg was chosen for computation, according to the classical design of the instrument.[10]

Figure 3 shows that both the determinant computed for any value of y at a given wavelength and the determinant calculated for any value of λ at an arbitrary y are not constantly zero over the definition interval.

As a consequence, we may infer that the functions $[1, m(y), n(y), p(y)]$ are linearly independent over the entire range of y and for any given λ. The only combination ΔI, ΔQ, ΔU, ΔV able to satisfy Eq. (18) is (0, 0, 0, 0). As a consequence, the two incoming Stokes vectors must be equal ($\mathbf{S}_{in1} = \mathbf{S}_{in2}$) fact which contradicts the hypothesis [Eq. (16)].

In conclusion, for each incoming, Stokes vector will correspond a different pattern of the intensity on the detector plane. Subsequently, it will be impossible to obtain the same output from two different incoming polarizations. Nevertheless, the use of a different material, a different configuration, or a particular binning procedure will require all the time the computation of this test for the uniqueness of the solution.

4 Impact of Noise

As a matter of fact, the measurements realized with a real device will be impacted by noise. The sources of noise are diverse, including many effects as photon counting, detector readout, and dark current. The previous derivation giving the uniqueness of the solution was performed in an ideal case exempt of noise. The question then is: how do noise perturbations in the signal impact the quality of results and the inversion process? In this paper, we will consider that the difference between the measured intensity and the theoretically predicted value will be mainly generated by the photon noise. The corresponding distribution is Poissonian, but can be assimilated to a Gaussian distribution in the (usual) case of a large number of photons.[19] Hence, its effects

on the quality of the extraction of the Stokes parameters can then be easily statistically estimated.[20,21]

In order to evaluate the impact of noise on the Stokes parameters retrieval through the inversion process, a random value σ is applied on the output signal. The variation range of σ defines the level of noise. Through the triple prism modulator and the grating, the light intensity (y axis) at any wavelength (x axis) projected on the detector plane is

$$I_{\text{out}}^{\text{meas}}(y_j) = I_{\text{out}}^{0}(y_j) + \sigma(y_j), \tag{21}$$

where $I_{\text{out}}^{\text{meas}}(y_j)$ is the noise impacted intensity at the position y_j on vertical, $I_{\text{out}}^{0}(y_j)$ is the corresponding analytical signal [Eq. (13)], and $\sigma(y_j)$ is the random noise on any elementary pixel.

Applying the least-squares fit method to Eq. (21), the uncertainties on the Stokes parameters can be computed.[21] This procedure provides information about the quality of the extraction of the Stokes parameters, for a given configuration of the system and of the modulation scheme. In order to compare between different configurations of the polarimeter (orientation of the analyzer and apex angles), the concept of efficiency of the modulation scheme, developed by del Toro Iniesta[8,19,22] and Collados[23,24] can be used. Both analyses are developed hereafter.

The function of merit of the fit is a chi-square function:

$$\begin{aligned}\chi^2(I,Q,U,V) &= \sum_{j=1}^{N}\left[\frac{I_{\text{out}}^{\text{meas}}(y_j) - I_{\text{out}}^{0}(y_j)}{\sigma(y_j)}\right]^2 \\ &= \sum_{j=1}^{N}\left\{\frac{I_{\text{out}}^{\text{meas}}(y_j) - \frac{1}{2}[I + Qm(y_j) + Un(y_j) + Vp(y_j)]}{\sigma(y_j)}\right\}^2.\end{aligned} \tag{22}$$

Minimizing this function with respect to I, Q, U, V parameters ($\frac{\partial\chi^2}{\partial S_i} = 0, S_i = I, Q, U, V$) provides the variances on the Stokes parameters. The partial derivatives yield immediately:

$$\underbrace{\frac{1}{2}\sum_{j=1}^{N}\begin{bmatrix} \frac{1}{\sigma^2(y_j)} & \frac{m(y_j)}{\sigma^2(y_j)} & \frac{n(y_j)}{\sigma^2(y_j)} & \frac{p(y_j)}{\sigma^2(y_j)} \\ \frac{m(y_j)}{\sigma^2(y_j)} & \frac{m^2(y_j)}{\sigma^2(y_j)} & \frac{m(y_j)n(y_j)}{\sigma^2(y_j)} & \frac{m(y_j)p(y_j)}{\sigma^2(y_j)} \\ \frac{n(y_j)}{\sigma^2(y_j)} & \frac{n(y_j)m(y_j)}{\sigma^2(y_j)} & \frac{n^2(y_j)}{\sigma^2(y_j)} & \frac{n(y_j)p(y_j)}{\sigma^2(y_j)} \\ \frac{p(y_j)}{\sigma^2(y_j)} & \frac{p(y_j)m(y_j)}{\sigma^2(y_j)} & \frac{p(y_j)n(y_j)}{\sigma^2(y_j)} & \frac{p^2(y_j)}{\sigma^2(y_j)} \end{bmatrix}}_{\mathbf{B}} \underbrace{\begin{pmatrix} I \\ Q \\ U \\ V \end{pmatrix}}_{\mathbf{S}} = \underbrace{\sum_{j=1}^{N}\begin{bmatrix} \frac{I_{\text{out}}^{\text{meas}}(y_j)}{\sigma^2(y_j)} \\ \frac{I_{\text{out}}^{\text{meas}}(y_j)m(y_j)}{\sigma^2(y_j)} \\ \frac{I_{\text{out}}^{\text{meas}}(y_j)n(y_j)}{\sigma^2(y_j)} \\ \frac{I_{\text{out}}^{\text{meas}}(y_j)p(y_j)}{\sigma^2(y_j)} \end{bmatrix}}_{\mathbf{R}}. \tag{23}$$

Using the contracted notation, this last system can be expressed as

$$\mathbf{B}\cdot\mathbf{S} = \mathbf{R}. \tag{24}$$

According to the least-squares fit method,[21] the variances corresponding to I, Q, U, and V are given by the diagonal elements of the matrix $\mathbf{B^{-1}}$:

$$\begin{cases} \sigma_1^2 = \sigma^2(I) = \mathbf{B_{11}^{-1}} \\ \sigma_2^2 = \sigma^2(Q) = \mathbf{B_{22}^{-1}} \\ \sigma_3^2 = \sigma^2(U) = \mathbf{B_{33}^{-1}} \\ \sigma_4^2 = \sigma^2(V) = \mathbf{B_{44}^{-1}} \end{cases}. \tag{25}$$

To compute the elements of the matrix $\mathbf{B}$, we will suppose that the noise $\sigma(y_j)$ is the same all along the vertical axis [$\sigma(y_j) = \sigma$]. Also we will consider that the uncertainty on the Stokes parameters is constant over the beam area.[9] This assumption is the natural consequence of the collimation of beam after the telescope assembly. Variations along the x and y axes could appear due to possible instrumental artifacts, and the calibration of the instrument would imply the knowledge of these variations and the correction. However, this topic is set aside from this paper.

The span of the summation from the system [Eq. (23)] N is driven by the Shannon–Nyquist theorem applied to the signal from Eq. (13) at a given wavelength. According to this theorem, the minimum sampling frequency should be at least twice the highest frequency contained in the signal or the Nyquist frequency. In terms of periods, measured along the y axis, we need to have

$$Y_s \leq \frac{Y_{\min}}{2}, \tag{26}$$

where Y_s is the sampling period and $Y_{\min}$ is the shortest period from the signal, corresponding to the Nyquist frequency.

Simultaneously, the sampling must cover at least the longest period of the signal ($Y_{\max}$). The value of $Y_{\min}$ thus provides information about the maximum size of a pixel (PS), PS $\leq Y_{\min}/2$, whereas $Y_{\max}$ represents the minimum height of the wedges and the detector. Using the Fourier transform, the frequencies from the signal provided by Eq. (13) can be found for any value of the wavelength and any architecture of the modulator. Figure 4 presents the dependency on the wavelength of the ratio $Y_{\min}/2$ and of the minimum height of the wedges $Y_{\max}$ for a modulator in MgF_2, with apex angles $(\xi, \psi) = (1.5 \text{ deg}, 3 \text{ deg})$.

To sample the signal at any wavelength in the transmission band of MgF_2, the size of the pixels must be smaller than the minimum of the curve from Fig. 4. This minimum occurs around $\lambda = 0.14$ μm and depends on the value of the apex angles. Therefore, for $(\xi, \psi) = (1.5 \text{ deg}, 3 \text{ deg})$, the pixels must be smaller than 64.5 μm, whereas for $(\xi, \psi) = (3 \text{ deg}, 1.8 \text{ deg})$ the value should be less than 59.3 μm.

The minimal height of the wedges (and of the detector), which can be inferred from the $Y_{\max}$ variation, depends on the chosen waveband and the apex angles.

For instance, in order to cover the spectral band 0.12 to 0.3 μm, the prisms (and the detector) must be at least 0.9 mm high, whereas covering the entire transmission window of MgF_2 will require at least 4.6 cm, in the case of the first geometry, $(\xi, \psi) = (1.5 \text{ deg}, 3 \text{ deg})$. For the second geometry, $(\xi, \psi) = (3 \text{ deg}, 1.8 \text{ deg})$, the minimum height is of about 1.14 mm at $\lambda = 0.3$ μm and 5.5 cm at 7 μm.

As long as $Y_{\min}/2 \geq 2$ PS, multiple equations [Eq. (13)] can be used to cover a $Y_{\min}/2$ distance [see Fig. 5]. This will increase the precision of the interpolation. Overall, for a detector of height $h = N_{\text{px}} \cdot \text{PS} \geq Y_{\max}(\lambda)$, where N_{px} is the total number of pixels from a column of the detector, a number of $N = N_{\text{px}}/n$ equations can be associated, where $n = 1,2...$ represents the number of pixels used to build a single equation [Eq. (13)]. If $n = 1$ brings the highest precision, a value bigger than 1 may significantly reduce the computation time.

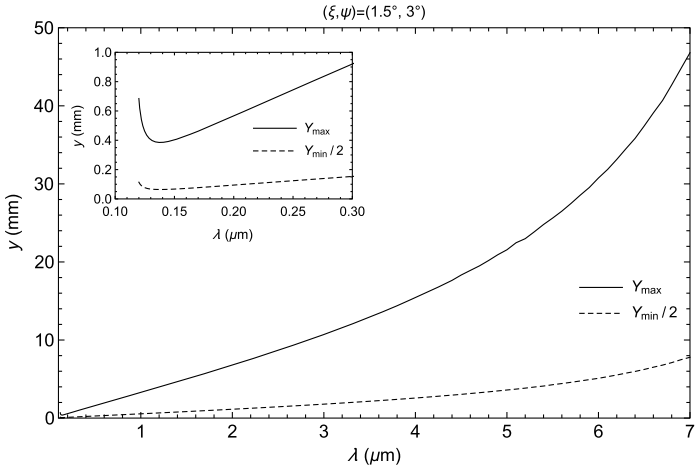

Fig. 4 Variation with the wavelength of the ratio $Y_{\min}/2$ corresponding to the maximum pixel size, and of the minimal height of the wedges $Y_{\max}$ for a modulator in MgF_2, with the apex angles $(\xi, \psi) = (1.5 \text{ deg}, 3 \text{ deg})$. The covered spectral band (0.12 to 7 μm) corresponds to the entire transmission window of MgF_2. The small graphic from top-left presents a zoom on the region 0.12 to 0.3 μm, where the minima of the curves are located.

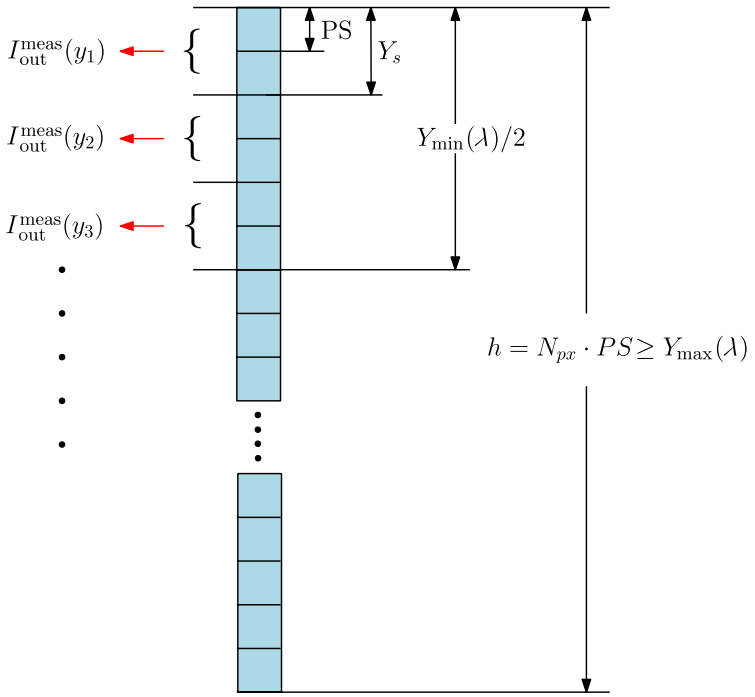

Fig. 5 Each measurement of the intensity $I_{\text{out}}^{\text{meas}}(y_j)$ corresponds to a number of n pixels, with $n \cdot \text{PS} \leq Y_{\text{min}}/2$, where Y_{min} is the minimum sampling distance resulting from the Nyquist theorem, and PS is the size of a pixel. In practice, the $Y_{\text{min}}/2$ of the structure presented above, based on MgF_2, is around 59.4 μm for a modulator with apex angles $(\xi, \psi) = (3\ \text{deg}, 1.8\ \text{deg})$ and about 64.5 μm for $(\xi, \psi) = (1.5\ \text{deg}, 3\ \text{deg})$. Considering the particular case of the UV domain, these values are above the common pixel sizes used in this range, situated between 10 and 25 μm. This allows the combination of multiple number of pixels in the construction of the modulation scheme. In this figure, the situation having $n = 2$ was depicted.

No matter the value of n, Eq. (21) and all the relations resulting from it must be integrated on the considered number of pixels n.

Assuming that the uncertainty affecting the detected intensity is the same along a column of the detector,[9] $\sigma(y_j) = \sigma$, then the matrix $\mathbf{B}$ can be written as

$$\mathbf{B} = \frac{1}{2}\frac{1}{\sigma^2}\sum_{j=1}^{N}\underbrace{\begin{bmatrix} 1 & m(y_j) & n(y_j) & p(y_j) \\ m(y_j) & m^2(y_j) & m(y_j)n(y_j) & m(y_j)p(y_j) \\ n(y_j) & n(y_j)m(y_j) & n^2(y_j) & n(y_j)p(y_j) \\ p(y_j) & p(y_j)m(y_j) & p(y_j)n(y_j) & p^2(y_j) \end{bmatrix}}_{\mathbf{C}}. \tag{27}$$

Therefore, we have directly

$$\mathbf{B}^{-1} = 2\sigma^2\mathbf{C}^{-1} \tag{28}$$

and from Eqs. (25) and (28)

$$\sigma_i = \sigma\sqrt{2\mathbf{C}_{ii}^{-1}}, \tag{29}$$

where $\mathbf{C}_{ii}^{-1}$ are the diagonal elements of the matrix $\mathbf{C}^{-1}$, and $i = 1,2,3,4$, corresponding to I, Q, U, V parameters.

The ratios σ_i/σ can be then plotted for different configurations of the modulator and various orientations of the analyzer. For instance, with a sampling distance of 10 μm (corresponding to

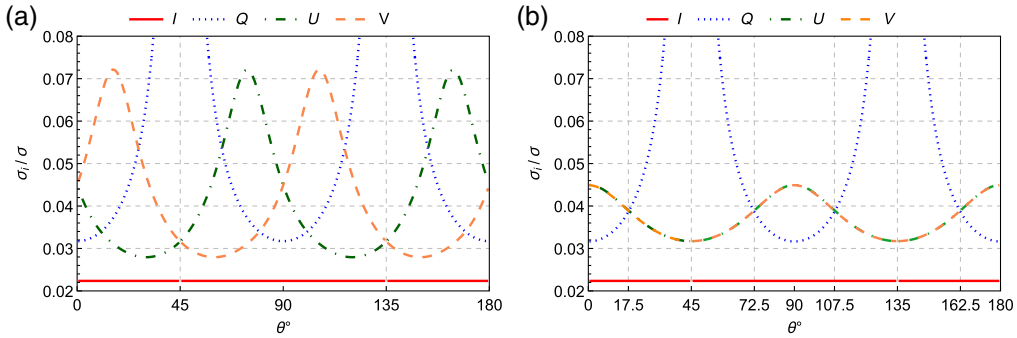

Fig. 6 Variation of the ratio σ_i/σ, between the uncertainty on the Stokes parameters and the uncertainty on the measured intensity, as a function of the orientation of the analyzer (the angle θ). (a) The "classical" case of a modulator,[10] with apex angles $\xi = 1.5$ deg, $\psi = 3$ deg and (b) a new geometry having $\xi = 3$ deg, $\psi = 1.8$ deg was considered. A uniform uncertainty along the y axis, on a wavelength of 0.125 μm, is assumed for the detected intensity and the Stokes parameters. The particular case of an MgF_2 medium was considered.

Table 1 Minimal and maximal values of uncertainties on Stokes parameters.

	$(\xi, \psi) = (1.5 \text{ deg}, 3 \text{ deg})$		$(\xi, \psi) = (3 \text{ deg}, 1.8 \text{ deg})$	
σ_I	$\frac{1}{\sqrt{N}}$		$\frac{1}{\sqrt{N}}$	
	Min	Max	Min	Max
σ_Q	$\frac{1.45}{\sqrt{N}}$	∞	$\frac{1.45}{\sqrt{N}}$	∞
$\sigma_{U,V}$	$\frac{1.27}{\sqrt{N}}$	$\frac{3.27}{\sqrt{N}}$	$\frac{1.45}{\sqrt{N}}$	$\frac{2}{\sqrt{N}}$

the approximate size of a pixel) and a column of $N = 2000$ pixels, the variations from Fig. 6 can be obtained for two different configurations of a modulator in MgF_2.

As it was expected, the I uncertainty is independent of the orientation of the analyzer, whereas the rest of the Stokes parameters are closely related to this angle. Thereby, for two specific analyzer orientations, 45 deg and 135 deg, the **B** matrix is no longer invertible because all the terms containing the $m(y)$ function are zero, as it can be noticed from Eqs. (13) and (14). This leads to an indetermination of the Q parameter.

Apart from the orientation of the analyzer, the general geometry of the modulator also plays an important role in the spectropolarimeter performances. Figure 6 presents the results for two different configurations. Each of them is associated with a different couple (ξ, ψ) representing the apex angles of the modulator (see Fig. 1). At left, the "classical" case[10] of a modulator with $(\xi, \psi) = (1.5 \text{ deg}, 3 \text{ deg})$ was plotted, whereas at right a case having $(\xi, \psi) = (3 \text{ deg}, 1.8 \text{ deg})$ was considered. We notice, in the second configuration, that similar values of the uncertainty on Q, U and V parameters can be obtained for orientations of the analyzer at 17.5 deg and 72.5 deg, 107.5 deg and 162.5 deg, respectively. In contrast, the first scenario has no intersection points for all the three parameters. The couples (ξ, ψ) able to minimize the uncertainties on the Stokes parameters can be derived through the study of the efficiency of the modulation scheme. The minimal and the maximal values of the ratio σ_i/σ corresponding to the studied cased are presented in Table 1.

Despite the periodical variation, the average level of this ratio remains close to the ideal one,[9] $1/\sqrt{N}$, in both cases (the red horizontal lines in Fig. 6).

5 Efficiency of the Modulation

Because the working principle of this spectropolarimeter is based on the continuous phase variation of the outgoing rays on the vertical direction, theoretically an infinite number of equations

[Eq. (15)] can be built on the y axis to help retrieve the incoming polarization. Practically, a limited number must be used, given the finite height of a detector and the pixel size. The questions about the appropriate number of equations, the best integration distance, and the best geometry of the modulator can be answered with the help of the concept of efficiency of the modulation scheme, as it was defined by del Toro Iniesta[8,22] and Collados.[23,24] Simultaneously, a comparison of this concept of spectropolarimeter with existing instruments can be inferred from the computation of the efficiency.

The system [Eq. (15)], describing the modulation scheme of the spectropolarimeter, can be rewritten under a matrix form as

$$\underbrace{\begin{bmatrix} I_{\text{out}}(y_1) \\ I_{\text{out}}(y_2) \\ \cdots\cdots \\ I_{\text{out}}(y_N) \end{bmatrix}}_{\mathbf{I}_{\text{out}}} = \frac{1}{2} \underbrace{\begin{bmatrix} 1 & m(y_1) & n(y_1) & p(y_1) \\ 1 & m(y_2) & n(y_2) & p(y_2) \\ \cdots & \cdots & \cdots & \cdots \\ 1 & m(y_N) & n(y_N) & p(y_N) \end{bmatrix}}_{\mathbf{O}} \cdot \underbrace{\begin{pmatrix} I_{\text{in}} \\ Q_{\text{in}} \\ U_{\text{in}} \\ V_{\text{in}} \end{pmatrix}}_{\mathbf{S}_{\text{in}}}, \tag{30}$$

or

$$\mathbf{I}_{\text{out}} = \mathbf{O} \cdot \mathbf{S}_{\text{in}}, \tag{31}$$

where $\mathbf{O}$ is the modulation matrix. Therefore

$$\mathbf{S}_{\text{in}} = \mathbf{O}^{-1} \cdot \mathbf{I}_{\text{out}}, \tag{32}$$

where $\mathbf{O}^{-1}$ is the demodulation matrix (also written as $\mathbf{D}$).

As described in Sec. 4 (Fig. 4), the detector plane is subdivided into N integration intervals, leading to N equations in the modulation scheme. If $N > 4$, then the matrix $\mathbf{O}$ is no longer easily invertible, and a pseudoinverse matrix must be used:[8,19]

$$\mathbf{D} = (\mathbf{O}^{\text{T}}\mathbf{O})^{-1}\mathbf{O}^{\text{T}}. \tag{33}$$

This works as a left-inverse matrix ($\mathbf{D} \cdot \mathbf{O} = 1$). The notion of the efficiency of the modulation as presented by del Toro Iniesta[8] can be then introduced

$$\epsilon_i = \left(N \sum_{j=1}^{N} \mathbf{D}_{ij}^2 \right)^{-\frac{1}{2}} \quad i = 1,2,3,4, \tag{34}$$

where i corresponds to each of the Stokes parameters. The four terms vector ϵ_i provides simultaneously information about the "quality" of the extraction of the Stokes parameters and the modulation scheme (the matrix $\mathbf{O}$). The total efficiency of the modulation scheme is defined by

$$\epsilon = \sqrt{\epsilon_2^2 + \epsilon_3^2 + \epsilon_4^2}. \tag{35}$$

The maximum reachable efficiency is 1 and is given by the configuration $\epsilon_i = \frac{1}{\sqrt{3}}$ for $i = 2,3,4$.

The concept of efficiency is also closely related to the uncertainty on the Stokes parameters. Indeed, from Eq. (32), we have that

$$\mathbf{S}_{\text{in}}(i) = \sum_{j=1}^{N} \mathbf{D}_{ij} \mathbf{I}_{\text{out}}(j) \quad i = 1,2,3,4. \tag{36}$$

Applying the propagation of errors, we obtain

$$\sigma_i^2 = \sigma^2 \sum_{j=1}^{N} \mathbf{D}_{ij}^2, \tag{37}$$

where σ_i is the uncertainty characterizing each of the Stokes parameters, and σ is the error related to each of the values $I_{\text{out}}(y_j)$, supposed to be the same for all the vertical pixels (or pixel compounds, if several are grouped). Combined to Eq. (34), this yields

$$\frac{\sigma_i}{\sigma} = \frac{1}{\epsilon_i \sqrt{N}}. \tag{38}$$

Therefore, the efficiency of the extraction of the Stokes parameters is nothing else but the inverse of the corresponding uncertainty. Any variation of the efficiency is then translated into a variation of the uncertainty. Higher is the efficiency for a parameter, lower is the uncertainty characterizing it and the more it constitutes a better choice for the modulation matrix. However, finding the best modulation matrix is not straightforward.

An essential role in the optimization of the modulation scheme is played by the number of equations N and by the number of pixels n used for each equation of the system [Eq. (15)]. This aspect can be easily proved by observing the evolution of the total efficiency as a function of N, for different values of n (Fig. 7).

A small integration step ensures a quicker retrieval of the highest efficiency, lowering the computation time.

The impact of the orientation of the analyzer on the quality of the extraction of the Stokes parameters, already observed in the case of the uncertainty, can be retrieved as well in the case of the efficiency.

Figure 8 shows the variation of the efficiency for each Stokes parameters with the orientation of the analyzer for a modulation scheme, in which 2000 integration intervals were considered with a pixel size $\Delta y = 10$ μm. In order to illustrate the impact of the apex angles, two configurations are presented: $(\xi, \psi) = (1.5 \text{ deg}, 3 \text{ deg})$, and $(\xi, \psi) = (3 \text{ deg}, 1.8 \text{ deg})$. Overall, the total efficiency of the system is around 0.99. This value is above classical cases sush as ZIMPOL—Zurich Imaging Polarimeter (0.72), ASP—Advanced Stokes Polarimeter (0.88), or TIP—Tenerife Infrared Polarimeter (0.92)[8,24] and proves that the studied model can be an important candidate at least for the astronomical observation. Also for a modulator with the apex angles $(\xi, \psi) = (3 \text{ deg}, 1.8 \text{ deg})$, it can be noticed that orientations of the analyzer at 17.5 deg, 72.5 deg, 107.5 deg, or 162.5 deg the efficiency of Q, U and V is around 0.574, very close to the ideal value of $\frac{1}{\sqrt{3}} = 0.577$.

In order to keep a high level of the efficiency and thus a low level of the uncertainty, the couple (ξ, ψ) must be chosen so that the two angles are not multiple one of another (Fig. 9):

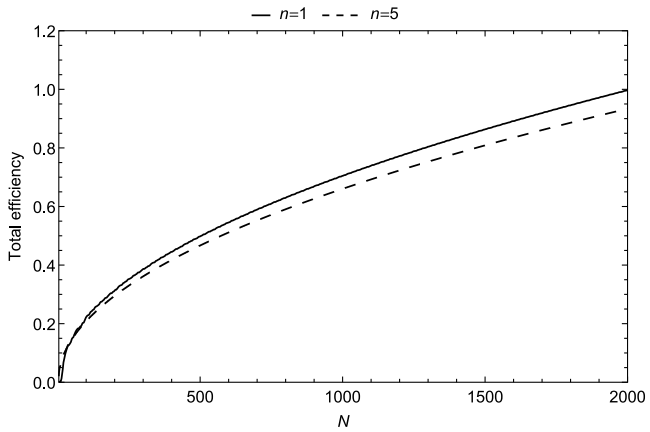

Fig. 7 Variation of the total efficiency for a modulator in MgF_2 with $(\xi, \psi) = (3 \text{ deg}, 1.8 \text{ deg})$ and $\theta = 72.5$ deg with respect to the number of equations from the modulation scheme and for two choices of pixel compounding, n. The continuous line corresponds to an integration pixel by pixel ($n = 1$, $N_{\text{px}} = N$) and the dashed line to an integration on compounds of five pixels ($n = 5$, $N_{\text{px}} = 5N$). The size of a pixel was considered here as being around 10 μm and the wavelength $\lambda = 0.125$ μm.

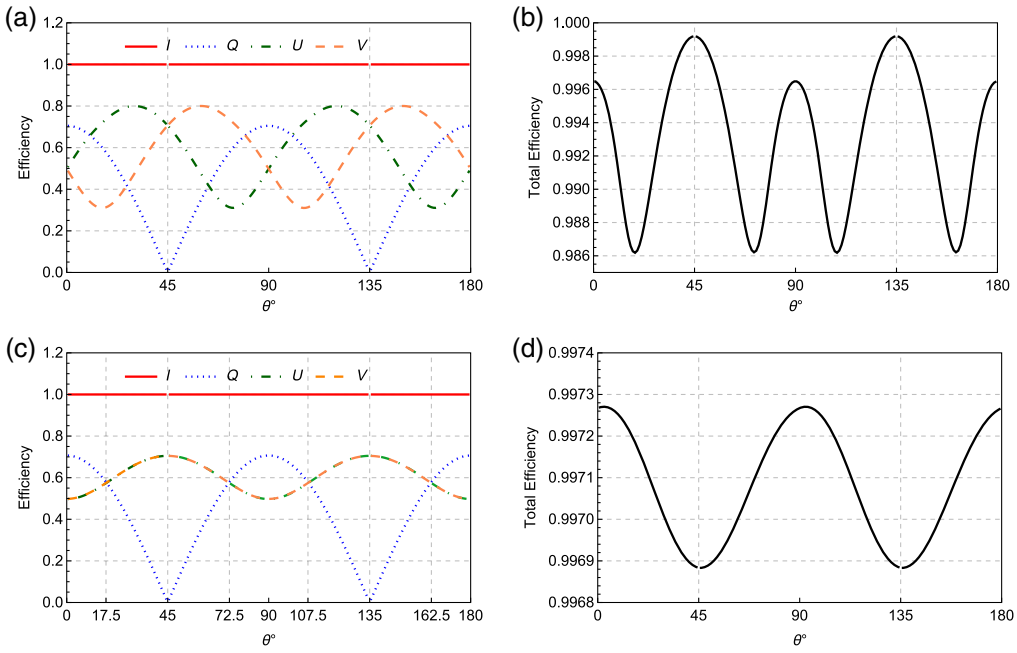

Fig. 8 Efficiency of the extraction for each of the Stokes parameters and total efficiency as a function of the orientation of the analyzer θ for two combinations of the apex angles (ξ, ψ). For $\xi = 1.5$ deg and $\psi = 3$ deg, (a), (b) the variations of the efficiencies of the extraction of Q, U, and V are following different patterns. There is no common maximum. Nevertheless, a (c), (d) different combination of the apex angles permits to have the same efficiency for U and V. Because the Q term is modulated only by the function $m[\theta, \Delta\phi_3(\psi)]$, varying the couple (ξ, ψ) does not impact the corresponding efficiency. The particular case of $\lambda = 0.125$ μm, $N = 2000$, and $\Delta n(\lambda)$ corresponding to MgF_2 was considered.

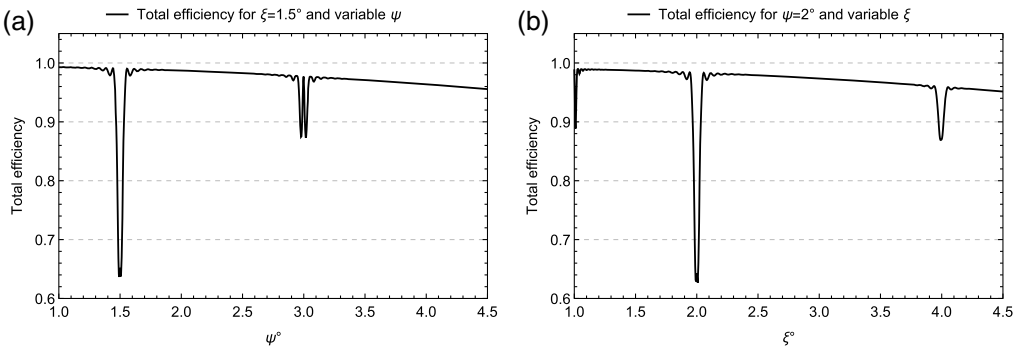

Fig. 9 The variation of the efficiency of the modulation scheme as a function of the apex angles. (a) For a fixed value of $\xi = 1.5$ deg, the angle ψ varies between 1 deg and 4.5 deg. It is noticeable the drop of the efficiency for $\psi = 1.5$ deg and around 3 deg. (b) $\psi = 2$ deg and ξ varies between 1 deg and 4.5 deg. Again, drops of the efficiency are observed at $\xi = k\psi$, $k = 1,2$.

$$\begin{cases} \text{a) for a given } \xi : \psi \neq k\xi, \ k = 1,2,\ldots \forall\ \xi \\ \text{b) for a given } \psi : \xi \neq k\psi, \ k = 1,2,\ldots \forall\ \psi \end{cases}. \tag{39}$$

Indeed, if the values of ξ and ψ are multiple one of another, then the nondiagonal terms of the matrix $A = O^{\mathrm{T}}O$ are maximized, and because of this the O matrix is not an optimal matrix of the modulation.[8] Again, just like in the case of the variation with the orientation of the analyzer (Fig. 8), the concept of efficiency is a good method to asses the best geometry of the modulator.

6 Conclusions

This mostly theoretical description of the STAS concept has shown that in ideal conditions, exempted of noise, such a device does not interfere with the polarization states: it is impossible to obtain the same pattern of intensity from different states of polarization.

Nevertheless, when the noise is added to the nominal signal, the determination of any incoming polarization is accompanied by uncertainty. By mapping the uncertainty on the Stokes parameters with respect to the orientation of the analyzer, it has been shown that angles like 45 deg and 135 deg should be avoided as they are erasing any information about the Q parameter of the incoming light. Apart from the orientation of the analyzer, the couple of angles (ξ, ψ) also plays an important role in the precision of measurements. Therefore, a geometry with $(\xi, \psi) = (3 \text{ deg}, 1.8 \text{ deg})$ can provide equal values of the uncertainties on the Stokes parameters for orientations of the analyzer at 17.5 deg, 72.5 deg, 107.5 deg, 162.5 deg. The level of uncertainty corresponding to these positions is 1.73 times higher than in the ideal case of a polarimeter, but it represents a compromise in which all Stokes parameters are determined with similar low errors (choosing other angles may improve the situation for one parameter, but degrade it for another).

Because this type of spectropolarimeter is based on the continuous variation of the phase on the vertical direction, multiple modulation schemes can be imagined. One of the best criteria to choose among them is the efficiency of the extraction of the Stokes parameters. In this paper, was investigated the dependency of the efficiency on the orientation of the analyzer and on the geometry of the modulator. Maxima of the total efficiency of about 0.99 are attainable, situating this concept of spectropolarimeter above classical examples such as ZIMPOL, ASP, or TIP. The impact of the apex angles on the efficiency has also proved that configurations of the type $\xi = k\psi$ or $\psi = k\xi$, where $k = 1,2,3,\ldots$ must be avoided.

Acknowledgments

The first author acknowledges the support of the STAR Institute and the Centre Spatial de Liège.

References

1. A. Morozhenko and A. Vid'machenko, *Polarimetry and Physics of Solar System Bodies*, Springer Science, pp. 369–384 (2005).
2. J.-L. Leroy, *La polarisation de la lumière et l'observation astronomique*, Editions des archives contemporaines, Paris (2001).
3. J. Bailey, L. Kedziora-Chudczer, and K. Bott, "Polarized radiative transfer in planetary atmospheres and the polarization of exoplanets," *Mon. Not. R. Astron. Soc.* **480**(2), 1613–1625 (2018).
4. L. C. G. Rossi and D. M. Stam, "Circular polarization signals of cloudy (exo)planets," *Astron. Astrophys.* **616**, A117 (2018).
5. L. Kolokolova, J. Hough, and A. C. Levasseur-Regourd, *Polarimetry of Stars and Planetary Systems*, Cambridge University Press, Cambridge (2015).
6. D. H. Goldstein, *Polarized Light*, CRC Press, Taylor & Francis Group, Boca Raton (2011).
7. E. Collett, *Field Guide to Polarization*, SPIE Press, Bellingham, Washington (2005).
8. J. C. del Toro Iniesta, *Introduction to Spectropolarimetry*, Cambridge University Press, Cambridge (2003).
9. W. Sparks et al., "Compact and robust method for full Stokes spectropolarimetry," *Appl. Opt.* **51**, 5495–5511 (2012).
10. M. Pertenais et al., "Static spectropolarimeter concept adapted to space conditions and wide spectrum constraints," *Appl. Opt.* **54**, 7377–7386 (2015).
11. M. Pertenais et al., "UVMag: space UV and visible spectropolarimetry," *Proc. SPIE* **9144**, 1017–1025 (2014).
12. M. J. Dodge, "Refractive properties of magnesium fluoride," *Appl. Opt.* **23**, 1980–1985 (1984).
13. H. H. Li, "Refractive index of alkaline earth halides and its wavelength and temperature derivatives," *J. Phys. Chem. Ref. Data* **9**, 161–290 (1980).

14. I. H. Malitson, "A redetermination of some optical properties of calcium fluoride," *Appl. Opt.* **2**, 1103–1107 (1963).
15. M. Daimond and A. Masumura, "High-accuracy measurements of the refractive index and its temperature coefficient of calcium fluoride in a wide wavelength range from 138 to 2326 nm," *Appl. Opt.* **41**(25), 5275–5281 (2002).
16. M. Pertenais, "Spectropolarimétrie stellaire UV et visible depuis l'espace," PhD thesis, Université Toulouse III—Paul Sabatier (2016).
17. E. W. Weisstein, "Wronskian," http://mathworld.wolfram.com/Wronskian.html (accessed 2019-20-05).
18. B. Borden, *Essential Mathematics for the Physical Sciences*, vol. I, Morgan & Claypool Publishers, San Rafael, California (2017).
19. C. U. Keller and F. Snik, "Polarimetry from the ground up," in *Solar Polarization*, R. S. V. Berdyugina and K. N. Nagendra, Eds., ASP Conference Series, vol. 405, pp. 371–382, Astronomical Society of the Pacific, San Francisco (2009).
20. D. A. Clarke, *Polarized Light and Optical Measurement*, International Series of Monographs in Natural Philosophy, vol. 35, Pergamon, Oxford (1971).
21. P. R. Bevington, *Data Reduction and Error Analysis for the Physical Sciences*, 3rd ed., McGraw-Hill Higher Education, Boston (2003).
22. J. C. del Toro Iniesta and V. M. Pillet, "Assessing the behavior of modern solar magnetographs and spectropolarimeters," *Astrophys. J. Suppl. Ser.* **201**, 22 (2012).
23. J. C. del Toro Iniesta and M. Collados, "Optimum modulation and demodulation matrices for solar polarimetry," *Appl. Opt.* **39**, 1637–1642 (2000).
24. M. Collados, "High resolution spectropolarimetry and magnetography," in *3rd Advances in Solar Physics Euroconference: Magnetic Fields and Oscillations*, B. Schmieder, A. Hofmann, and J. Staude, Eds., ASP Conference Series, vol. 184, 3–22, Astronomical Society of the Pacific (1999).

Bogdan Vasilescu received his BS degree in physics and his MS degree in space sciences from the University of Liège in 2016 and 2019, respectively. He is a PhD student at the Centre Spatial de Liège of the University of Liège. His current research is related to the development of a static imaging spectropolarimeter able to cover any type of polarization.

Biographies of the other authors are not available.